Applied Catalysis B: Environmental 188 (2016) 177–188

Contents lists available at ScienceDirect

Applied Catalysis B: Environmental

journal homepage: www.elsevier.com/locate/apcatb

Effective Diffusivity Measurement on a Monolithic Reactor using SPACI-MS Technique

Manish Sharma*, Mark Dearth

Ford Motor Company, Dearborn, MI, United States

ARTICLE INFO

Article history:
Received 17 August 2015
Received in revised form
25 November 2015
Accepted 19 January 2016
Available online 22 January 2016

Keywords:
Effective diffusivity measurement
Catalyst
Monolith
Washcoat
Spaci-MS
Porous materials

ABSTRACT

Measuring Effective Diffusivity in the pores of the catalytic washcoat of a monolith reactor is a challenging task. In this work, Spaci-MS technique has been used to measure effective diffusivity in the porous washcoat, and through the porous walls of the cordierite monolith substrate. A mixture of a tracer gas (in this case O_2) was introduced in a center (feed) channel along with a carrier gas, and the axial profile of tracer gas was measured in the neighboring channels. The axial profile of the tracer gas in the neighboring channels depends on the diffusivities in the gas phase, in the washcoat layer and through the substrate wall. A mass balance was made around the 1-adjacent channel to compare the calculated tracer profile with the measured profile, and used to get the value of effective diffusivity. Experiments were done on an uncoated (blank, substrate only) monolith to measure the effective diffusivity in the substrate, and then experiments were repeated for a washcoated monolith to measure the effective diffusivity in the catalytic washcoat layer. The experiments were also repeated at different temperatures to get the temperature dependence of the observed effective diffusivity. The results showed that the monolith substrate was in the bulk diffusion region and the washcoat exhibited Knudsen diffusion. Effective diffusivity of O_2 in substrate was calculated to be 9.28×10^{-6} m^2/s and in washcoat to be 2.2×10^{-6} m^2/s at 100 °C.

1. Introduction

The key to understanding transport processes in a porous medium or porous catalyst is the knowledge of effective diffusivity (D_{eff}) of the characteristic molecular species. Diffusional resistance is significant in many gas solid reactions under their operating conditions, such as reactions in zeolites. In automotive applications, the use of zeolites has led to the porous washcoat now generally consisting of macropores, mesopores and micropores, depending on the crystal/particle size in the washcoat. Due to this range of pore sizes, any of Knudsen, bulk or configurational diffusion may be significant. Diffusivity data for various reactant species is required to understand which transport/reaction process limits the extent of the reaction, and to improve reactor performance. Modern reactor design uses an accurate mathematical model of the reactor (with the porous catalyst) which requires an accurate estimate of the diffusivities. Pore size distribution and sizing of the porous catalyst can be optimized so that the diffusional resistances are as small as possible.

There are two kinds of diffusional regimes in pores, the bulk/molecular diffusion and the Knudsen diffusion. Effective diffusivity in a porous catalyst depends on its porosity and tortuosity. While porosity of a medium restricts the cross-sectional area available for transport; tortuosity characterizes the convoluted nature of the porous pathways followed by the diffusing species. Effective diffusivity can be written as

$$D_m = \frac{\varepsilon}{\tau} \times D_o \quad (1)$$

where D_m is the effective diffusivity, D_o is the reference/equivalent diffusivity, ε is the porosity of the material and τ is the tortuosity. In the Knudsen regime, the diffusivity is given by:

$$D_k = \frac{4}{3} K_o \left(\frac{8RT}{\pi M}\right)^{1/2} \quad (2)$$

where D_k is the Knudsen diffusivity, K_o is the Knudsen coefficient, R is the universal gas constant, T is the temperature and M is the Molecular weight of species. The combined reference diffusion coefficient is given by the Bosanquet formula:

$$D_o = \left(\frac{1}{D_b} + \frac{1}{D_k}\right)^{-1} \quad (3)$$

where D_b is the bulk diffusivity.

* Corresponding author.
E-mail addresses: msharm13@ford.com (M. Sharma), mdearth@ford.com (M. Dearth).

http://dx.doi.org/10.1016/j.apcatb.2016.01.048
0926-3373/

Nomenclature

C	Concentration in gas phase (mol/m^3)
D	Diffusivity (m^2/s)
k	Mass transfer coefficient (m/s)
K_o	Knudsen coefficient (m)
M	Molecular weight of gas species
R	The universal gas constant
R_Ω	Hydraulic radius (m)
t	Time (s)
T	Temperature (oC)
u	Linear velocity (m/s)
w	Wall thickness (m)
x	Length (m)
ε	Porosity
τ	Tortuosity
ρ	Density (g/m^3)

There are methods available in the literature to model effective diffusivity in multi-pore size materials [1]. Several methods have also been described to measure the effective diffusivity in the porous catalyst [2–4]. Richardson [2] describes a gas chromatographic method for measuring the effective diffusivity through a porous catalyst bed. A gas sampling valve is used to introduce a pulse of gas at the inlet, and the resulting broadening of the pulse as it passed through the bed was analyzed to get an estimate of effective diffusivity. This method is more useful for a large scale catalyst system. Richardson also found that upon catalyst fouling, the change in tortuosity was only 0.9, whereas the surface area changed by a factor of 5. A Wicke-Kallenbach cell is another frequently used system for a large scale catalyst, where a concentration gradient is applied across a catalyst pellet and effective diffusivity is determined from the concentration profiles (vs. time) on the two sides of the pellet. It offers an easy design and operation, but is not suitable for direct use in measuring effective diffusivities across a monolith wall. Beeckman [3] suggested a method to measure effective diffusivity through the wall of a specially built monolith channel. The diameter of the channel used was 6 mm (much larger than the channel diameter of monoliths used in automotive industry (less than 1 mm)) and was therefore easier to work with for their study. Hayes et al. [4] described how Beeckman's method can be modified to smaller diameter monoliths, but used a special system made of a 7 channel monolith, where the inlet channel was the center channel and the remaining 6 channels (called "out channels") surrounded the inlet channel. It also included a complicated system of adding gases in the inlet and outlet channels through separate connections, and trying to maintain zero pressure drop along the monolith wall. Additionally, it ignored any mass transfer to the outside of the system through the walls of the outer channels. The method described in this work does not need any special monolith. It can be used on any monolith sample available. It uses the SPACI-MS technique [5] to measure the concentrations in the inlet and outlet channels. Further it includes a more complete mass balance on the "adjacent to inlet" channels. The catalyst sample used is also much longer than the shorter (13 mm) sample used in previous studies to allow mass transfer across even a heavily coated monolith wall. The method shown in [6] is more suited to nanopores, and is computationally more intensive. It includes using Confocal Raman Spectroscopy to monitor mass transport and doing a rigorous numerical simulation using the boundary element method.

2. Experimental Methods

One inch (nominal) diameter sample of a cordierite monolith was removed from a full size casting using a diamond hole saw. The cores were typically 0.07 m (or more) in length and typically 0.97 in. in diameter after cutting. The catalyst sample was wrapped with a ceramic cloth to ensure a gas tight fit into a quartz reactor tube of 1 in. (nominal) I.D. The catalyst sample in the reactor tube was then mounted with stainless steel end caps to allow the gastight delivery of gaseous flow through the reactor tube and catalyst sample. Special fittings allow for the introduction of small diameter stainless steel capillary tubing into the reactor volume and to be inserted at various depths within the catalyst channels of the sample. These interface fittings were built from Swagelok™ fittings of various sizes and of configurations to allow the flow of both bulk gas and the movement of the capillary tubing (Fig. 1).

The uppermost capillary interface includes an inlet port for bulk carrier gas (N_2 at 12–15 L/min) and a capillary flow of O_2 at 20 mL/min or less. The upper (single) capillary delivering the O_2 tracer gas was positioned at the inlet of the catalyst sample in a center channel and approx. 0.5 mm into the front edge of the catalyst channel. The flow of tracer gas was controlled by a NIST certified calibrated mass flow controller (MKS) and a three way, fast-acting, micro switching valve. Tracer gas flow is vented to exhaust through the valve until such time as the experiment is started, when a digital signal is used to switch the valve and precisely record the switching event using a digital/analog interface control and Labview software (National Instruments) algorithms.

Three additional capillaries were inserted from the outlet side of the catalyst and reactor tube through an identical custom built interface that also allows the manipulation of these sampling capillaries. The trio of capillaries inserted from the outlet side of the reactor all terminate in a Swagelok assembly that also has sources of nitrogen diluent gas and a sample line connection to a V&F CIMS, a specialty mass spectrometer that uses charge exchange ionization to selectively ionize trace gases in the presence of bulk nitrogen gas [7,8].

The sampling capillary interface tubes were inserted into channels arranged around the center channel receiving the O_2 tracer gas, in three distinct patterns. Pattern 1 (1-Adjacent channels, as shown in Fig. 2) was where the gases were sampled in channels that shared an adjacent channel wall with the center channel receiving the tracer gas. Pattern 2 (Diagonal channels) is where all channels shared a corner with the center channel. Pattern 3 (2-Adjacent channels) is where the sample capillaries are one channel removed from the center channel, with 2 walls between the source channel and the measurement channel.

In a typical experiment the sampling capillaries would be inserted through the catalyst in individual channels, until their tips were observable flush with the front edge of the channels of the catalyst sample. A magnifying lens was used to observe and adjust them precisely to be flush with the leading edge of the catalyst. Once positioned, the gap between two fittings on the outlet capillary interface was measured with a Machinists digital caliper. As the sampling (outlet side) capillaries were repositioned during the measurement of the tracer gas diffusional concentration, the fitting gap was measured to determine the location of the assembly. A graphite Vespel ferrule in a Swagelok tube fitting allowed adjustment of the position of the MS sampling interface and the capillary tube inlet locations could be adjusted incrementally from the front face of the catalyst sample to its rear face with its location known within about 0.05 mm accuracy. The flowrates of the capillaries for both the inlet and the outlet interfaces were determined using a NIST certified bubble flowmeter (STEC) with an accuracy of + or −1% of reading. Gas temperatures were measured and controlled using a 1/32" type K thermocouple inserted into the front face of the

Fig. 1. Photos are described in numerical sequence: Photo 1. The inlet control system A. 1/16" swagelok interface fitting for tracer gas capillary introduction; B. bulk gas inlet port; C. microvalve for switching on/off tracer gas flow. Photo 2.The front face of the catalyst sample with; A tracer gas capillary and thermocouple inserted from front face side. B. Capillary sampling tubes protruding completely through the catalyst core from the downstream side. C. The front face of the catalyst sample. Photo 3. Location of the catalyst and capillaries in the tube furnace oven; A. Upstream side of catalyst. B catalyst centered in oven. C. Downstream side of oven. Photo 4. The outlet gas fittings detail; A. The bulk gas outlet. B. The capillary sampling assembly held by a graphite ferrule and Swagelok fitting. Photo 5. Adjustable section of the capillary sampling system. A. 1/8" o-ring sealed tubing fitting. B. 1/8" tube encasing the 0.350 mm O.D. capillaries. C. 1/8" o-ring seal adapter to ¼" tube. D. ¼" tube about 8" long. E. 1/16" to ¼" swagelok adapter fitting as terminus for the capillaries from the reactor volume. Photo 6. Capillary to CIMS interface; A. Capillary sampling tube connection. B. Tubing adapter from capillary to 1/8" fitting. C. Dilution gas inlet from mass flow controller (MFC not shown). D. Gas connection to CIMS vacuum system.

catalyst sample in parallel with and to the same nominal depth as the tracer gas capillary. The flow reactor and the region around the catalyst sample was suspended and centered in a Lindberg/Blue oven with a tube heating surface conforming to the shape of the quartz reactor tube and encompassing a region about 8" on either side of the catalyst volume.

The operation of the V&F Airsense CIMS has been described in detail elsewhere [7,8]. The concentration of the tracer gas in the adjacent channels was determined using a xenon/krypton mixture as a charge exchange ionization source. The analyte gas stream is introduced from the capillary interface into an interaction zone of the mass spectrometer and the resulting secondary ions are subsequently analyzed using quadruple mass spectrometry to very accurately and precisely measure the concentration of the analyte of interest, in this case O_2 in a bulk nitrogen gas stream. This measurement could be done with an extracted volume of about 20 mL/min (the sum of the gas flows from the three capillaries inserted around the center channel at various lengths downstream from the source). Post processing of the raw concentration data and the positional data was done in Excel.

It should be pointed out that the flow in the channels is not expected to be affected by the capillaries. The diameter of capillary is 0.350 mm O.D. and about 0.180 mm I.D. In contrast the hydraulic diameter of the monolith channel with a double washcoat layer is about 0.867 mm. The tracer gas flow rate is about 10 mL/min, while the sampling capillaries each take about 5–10 mL/min, which is small compared to the gas flow rate in each channel of about 66 mL/min.

Three monolith samples were used for evaluation; an uncoated high porosity (65% porosity) cordierite substrate, a substrate with

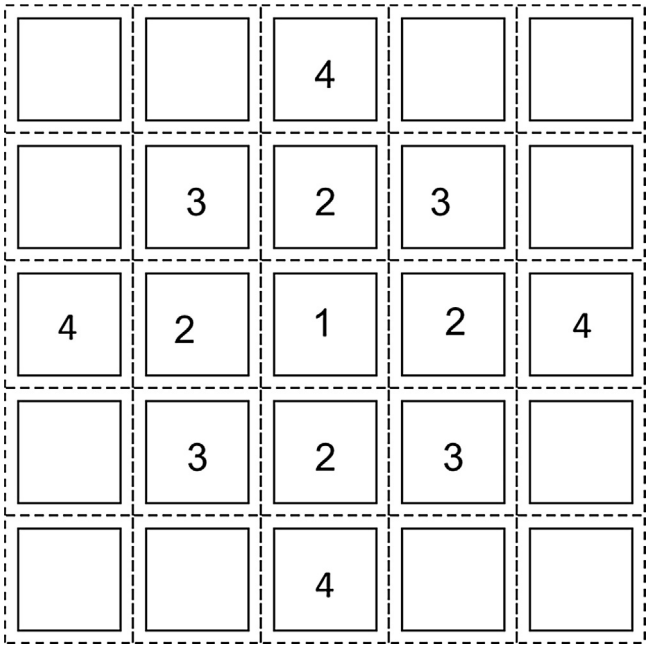

Fig. 2. Channel 1 is the inlet channel, channels labeled "2" are the 1-adjacent channels, channels labeled "3" are the diagonal channels and channels labeled "4" are the 2-adjacent channels. Channels labeled 2, 3 and 4 were sampled by MS.

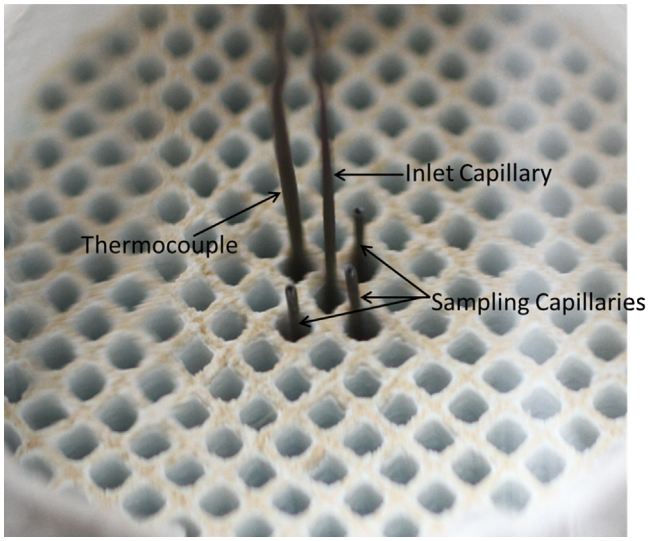

Fig. 3. Details of Photo 2 from Fig. 1; sampling capillaries from downstream side of catalyst are protruding above the front face of the sample (not their normal location) while the inlet capillary and the thermocouple are inserted downward into the catalyst channels from the inlet side (usually positioned just inside the catalyst channel).

a single layer of zeolite washcoat and a substrate with two layers (zeolite layers) of same washcoat. All samples were 300 cells per square inch monoliths, 1" nom. in dia. and 3" long, with a 12 mil wall thickness substrate. The washcoat loading on the single layer sample was 2.4 g per cubic inch (average washcoat thickness = 96.3 μm), while on the dual layer sample the washcoat loading was 3.6 g per cubic inch (average washcoat thickness = 96.3 + 62.7 μm). Both washcoat layers are made of beta zeolite. Other details of the washcoat are proprietary. As shown in Fig. 3, the tracer gas (O_2) is introduced in the center channel (Channel 1) and measurements of O_2 concentration at steady state are taken at different axial distances downstream in channel 2 (the adjacent channel), channel 3 (the diagonal channel) and channel 4 (the 2-adjacent channel). In every case, three capillaries, each in its own channel, are used to sample and an average of these three measurements is taken. For example to measure the concentration in channel 2, measurement capillaries are introduced in the three channels adjacent to channel 1 (see Fig. 3), and an average of the three readings is taken.

3. Experimental Results

Diffusion measurements were done at two temperatures, 100 and 200 °C. The inlet flow of tracer gas was set at a value near 10 mL/min of pure O_2 in the center channel and the total system flow in all cases was measured using a calibrated mass flow meter to be 13200 ± 1% mL/min. Fig. 4(a) shows the ppm measurements in the 1-adjacent (also called "adjacent"), diagonal and 2-adjacent channels of the substrate only sample at 100 °C, and Fig. 4(b) shows the same results at 200 °C. Measurement points were spaced to optimize the data collection to identify the concentration curves. More data points were taken in the adjacent and diagonal channels since more accuracy is needed in these channels for the analysis. The measured data points are plotted to get an idea of how the concentration profiles vary axially. As can be expected the O_2 concentration in the adjacent channel goes through a maximum. Initially the concentration rises with distance as more O_2 diffuses in the adjacent channel from the center inlet channel, but this also leads to a concentration difference between the adjacent channel, and the diagonal channels and the 2-adjacent channel, which share a common wall with the "adjacent channel". This leads to O_2 diffusing in the diagonal and 2 adjacent channels, and thus the O_2 concentration in the adjacent channel starts decreasing with distance. It should also be noted that the maximum concentration in the adjacent channel is reached at a shorter axial distance at the higher temperature, due to the increase in diffusivity with temperature. The concentration in the diagonal channel is higher than the concentration in the 2 adjacent channels, and also appears to show a maximum. Diagonal channels share 2 walls with the adjacent channel, while the 2-adjacent channels only share one wall with the adjacent channel. Thus diagonal channels get twice the O_2 amount diffused through the walls compared to the 2-adjacent channels. On the other hand the diagonal channels also start losing the O_2 through diffusion earlier since the rate of diffusion depends on the concentration gradient, leading to the diagonal channel O_2 concentration slightly dropping around 2 inch distance. Fig. 5(a) shows the ppm measurements in the adjacent, diagonal and 2-adjacent channels of the single washcoat layer sample at 100 °C, and Fig. 5(b) shows the same results at 200 °C. As expected the O_2 profiles are more delayed (shifted to the right) in the washcoated sample due to the extra diffusional resistance to "across the channel wall diffusion" caused by the washcoat layer. The maximum in the adjacent channel in Fig. 5(a) is at 1.5 in. compared to at 0.8 in. for uncoated substrate (Fig. 4(a)). Otherwise the data follows trends similar to ones discussed for Fig. 4(a) and (b). Finally, Fig. 6(a) shows the ppm measurements in the adjacent, diagonal and 2-adjacent channels of the dual washcoat layer sample at 100 °C, and Fig. 6(b) shows the same results at 200 °C.

4. Analysis and Discussion

The gas phase mass balance in the channel of a monolithic reactor can be written as:

$$\frac{\partial C_{g,i}}{\partial t} = -u\frac{\partial C_{g,i}}{\partial x} - \frac{k_m}{R_\Omega}(C_{g,i} - C_{s,i}) \quad (4)$$

where "C_g" is the concentration in the gas phase and "C_s" is the concentration at the solid wall, "u" is the linear velocity, "R_Ω 'is the

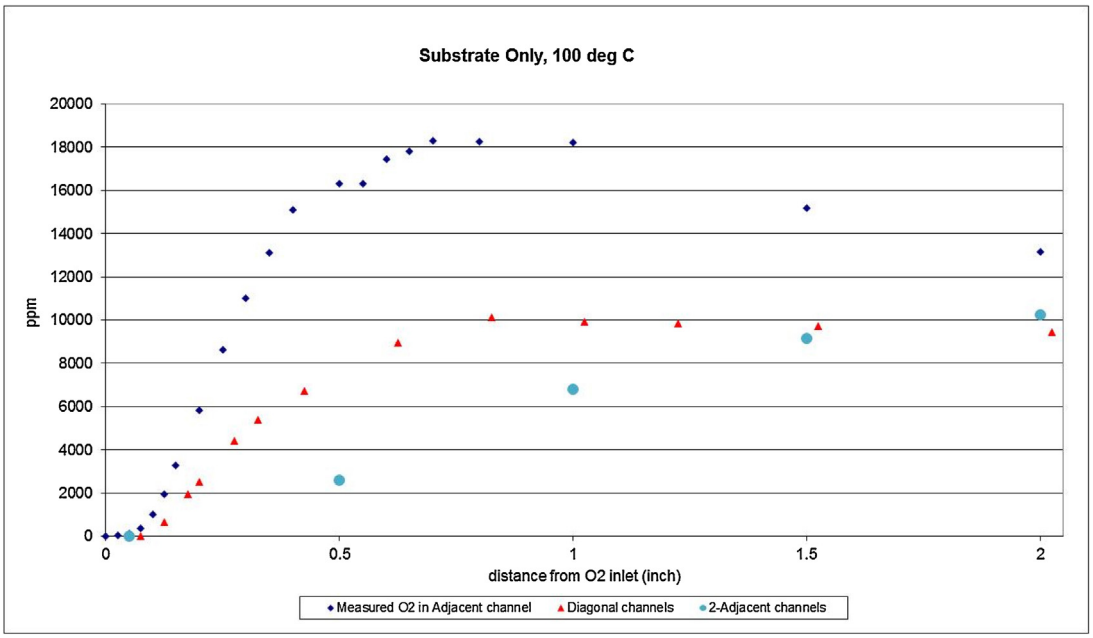

(a)

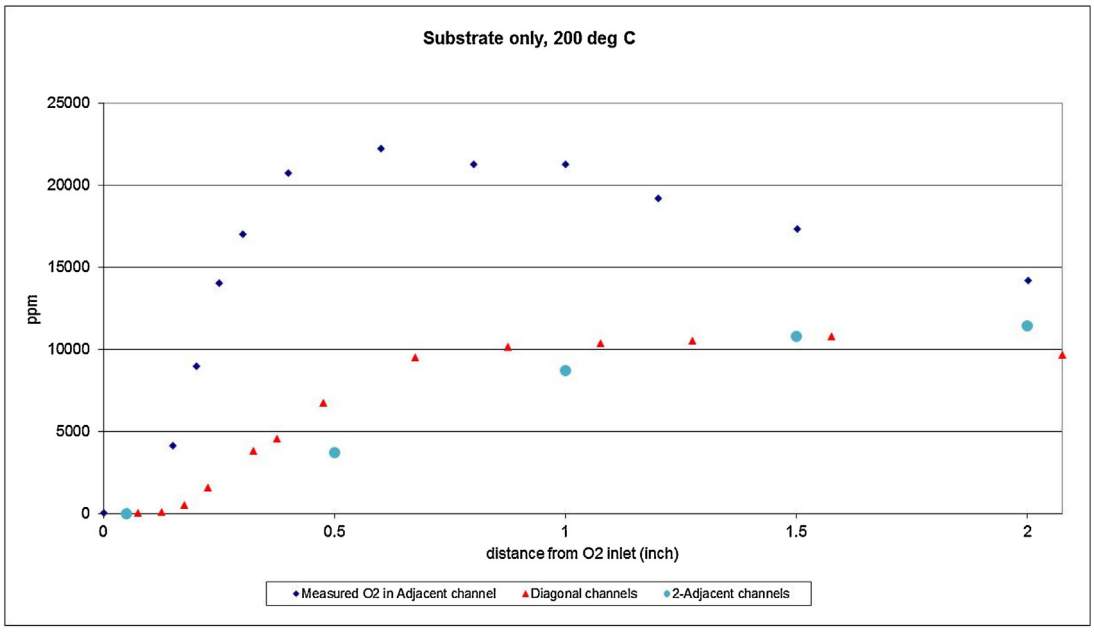

(b)

Fig. 4. Measured data (ppm) in the adjacent, diagonal and 2-adjacent channels of the substrate only sample at (a) 100 °C and (b) 200 °C vs axial distance from tracer gas inlet (inch).

channel hydraulic radius, and "k_m' is the mass transfer coefficient in the gas phase.

Also the mass flux balance in the transverse direction gives:

$$k_m(C_{g,i} - C_{s,i}) = k_{overall}(C_{g,1} - C_{g,2}) \quad (5)$$

where '$C_{g,1}$' is the gas phase cup mixing concentration in channel 1 and "$C_{g,2}$" is the gas phase cup mixing concentration in channel 2. Also, $k_{overall}$ (the overall mass transfer coefficient) is given by-

For substrate only sample:

$$\frac{1}{k_{overall}} = \frac{1}{k_m} + \frac{w_{sub}}{D_{sub}} + \frac{1}{k_m} \quad (6)$$

For the single washcoat layer sample:

$$\frac{1}{k_{overall}} = \frac{1}{k_m} + \frac{w_{sub}}{D_{sub}} + \frac{2 * w_{wash,1}}{D_{wash,1}} + \frac{1}{k_m} \quad (7)$$

For the dual washcoat layer sample:

$$\frac{1}{k_{overall}} = \frac{1}{k_m} + \frac{w_{sub}}{D_{sub}} + \frac{2 * w_{wash,1}}{D_{wash,1}} + \frac{2 * w_{wash,2}}{D_{wash,2}} + \frac{1}{k_m} \quad (8)$$

where "w_{sub}" is the thickness of the substrate, "D_{sub}' is the effective diffusivity in the substrate, "$w_{wash,1}$' is the thickness of the first washcoat layer, '$D_{wash,1}$" is the effective diffusivity in the first washcoat layer, "$w_{wash,2}$" is the thickness of the second washcoat layer, "$D_{wash,2}$" is the effective diffusivity in the second washcoat layer,

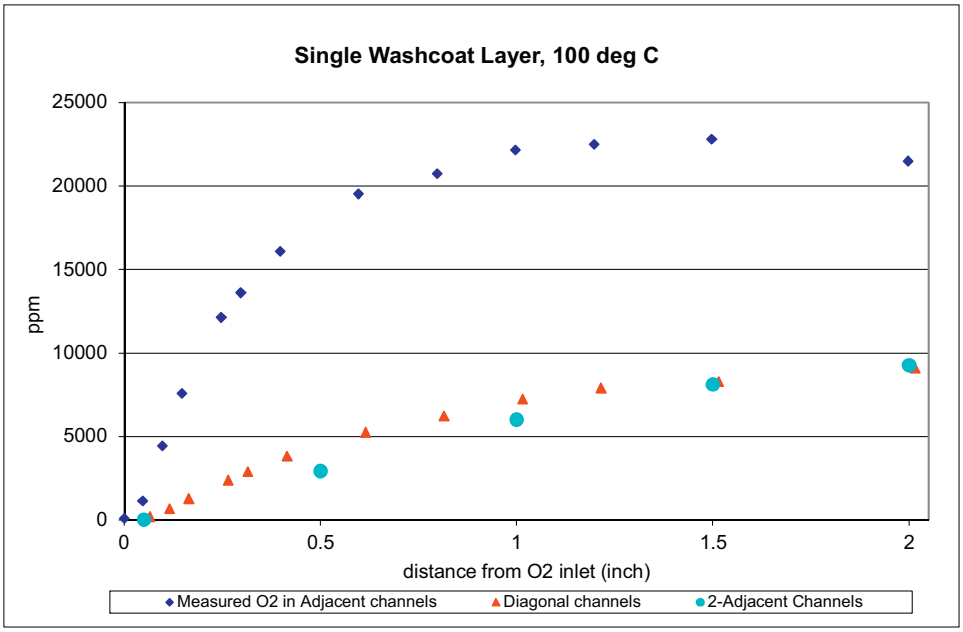

(a)

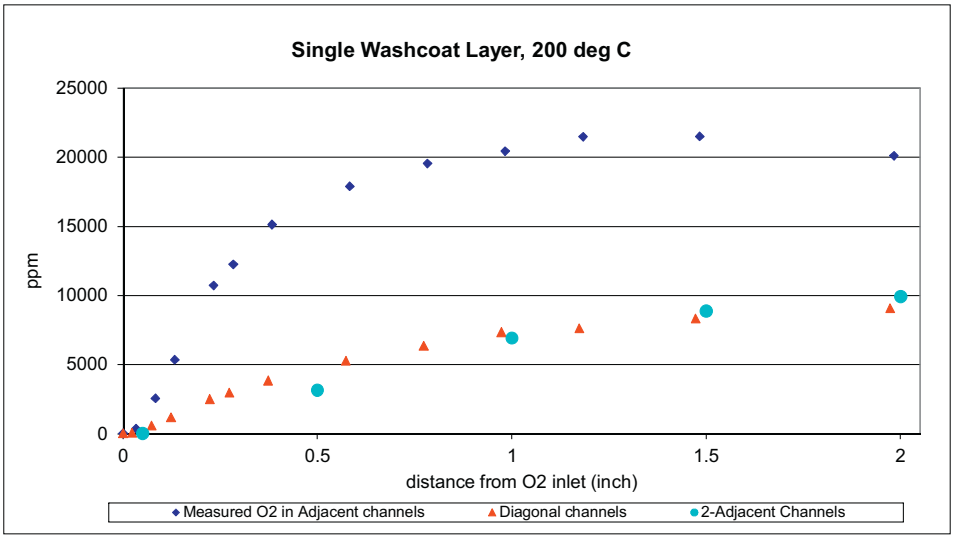

(b)

Fig. 5. Measured data (ppm) in the adjacent, diagonal and 2-adjacent channels of the single layer washcoat sample at (a) 100 °C and (b) 200 °C vs axial distance from tracer gas inlet (inch).

and "k_m' is the bulk mass transfer coefficient. For the dual washcoat layer catalyst, the first layer is the bottom layer and the second layer is the top layer.

Eqs. (4) and (5) can be combined to get

$$\frac{\partial C_{g,i}}{\partial t} = -u\frac{\partial C_{g,i}}{\partial x} - \frac{k_{overall}}{R_\Omega}(C_{g,1} - C_{g,2}) \quad (9)$$

At steady state, LHS (transient term) of Eq. (9) is zero. In order to derive the effective diffusivity in the uncoated monolith, data from Fig. 4(a) and 4(b) is used. The steps described below are used for calculations.

1. First, the adjacent, diagonal and 2-adjacent channel data are aligned axially using interpolation in MS Excel.
2. Since the feed concentration of O_2 in the inlet channel is known and $C_{g,2}$, the gas phase O_2 concentration in the adjacent channel is also known, concentration in the inlet channel (along axial distance) can be calculated using Eq. (9) (at steady state) as a function of $k_{overall}$. Gas phase bulk diffusivity of oxygen and substrate thickness are also known (Table 1).
3. Next making a mass balance around adjacent channel (which shares walls with inlet, diagonal and 2-adjacent channels, see channel 2 in Fig. 2), concentration in adjacent channel as a function of $k_{overall}$ is calculated (using Eq. (9) at steady state) and compared with measured values at different axial distances.
4. $k_{overall}$ is varied to minimize the sum of square of differences between calculated and measured O_2 concentration values in the adjacent channel. The best value of $k_{overall}$ (least sum of square of

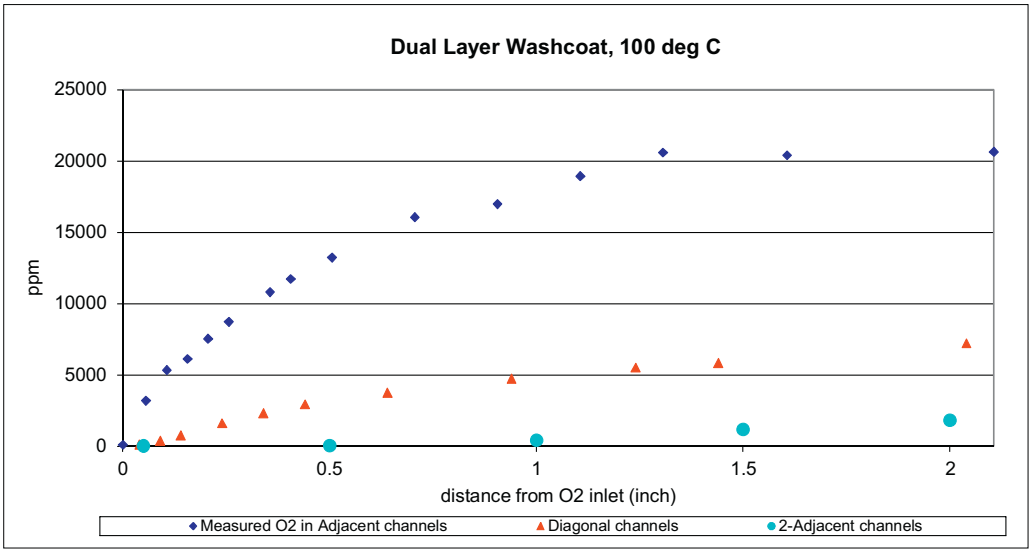

(a)

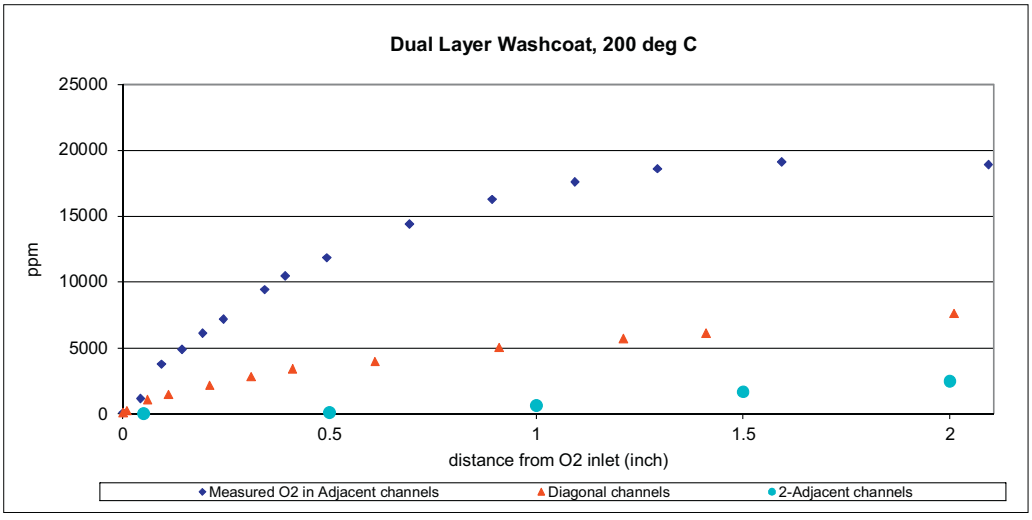

(b)

Fig. 6. Measured data (ppm) in the adjacent, diagonal and 2-adjacent channels of the dual layer washcoat sample at (a) 100 °C and (b) 200 °C vs axial distance from tracer gas inlet (inch).

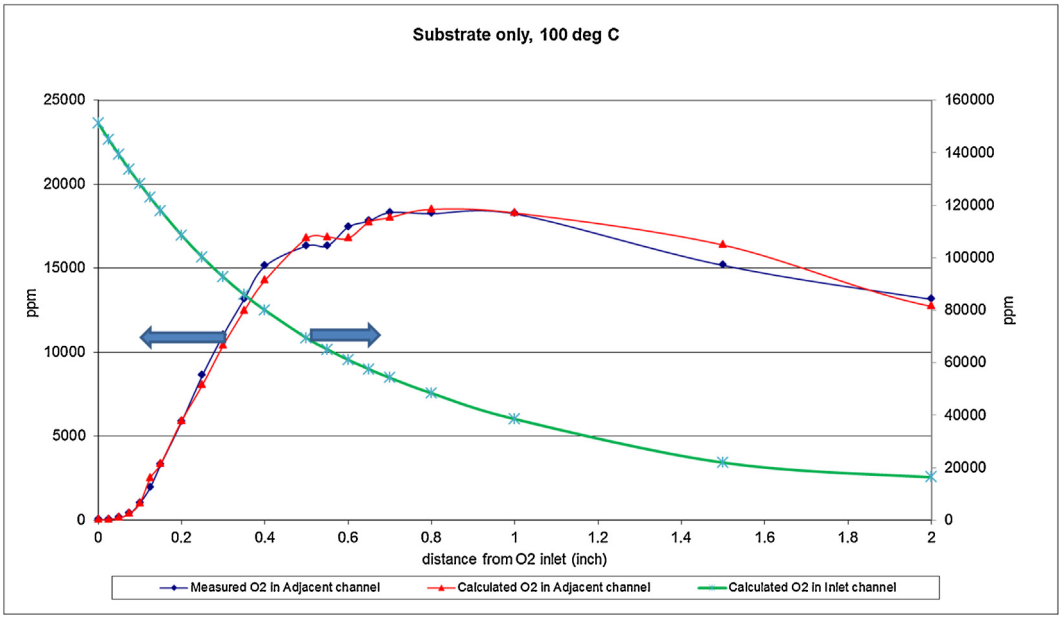

(a)

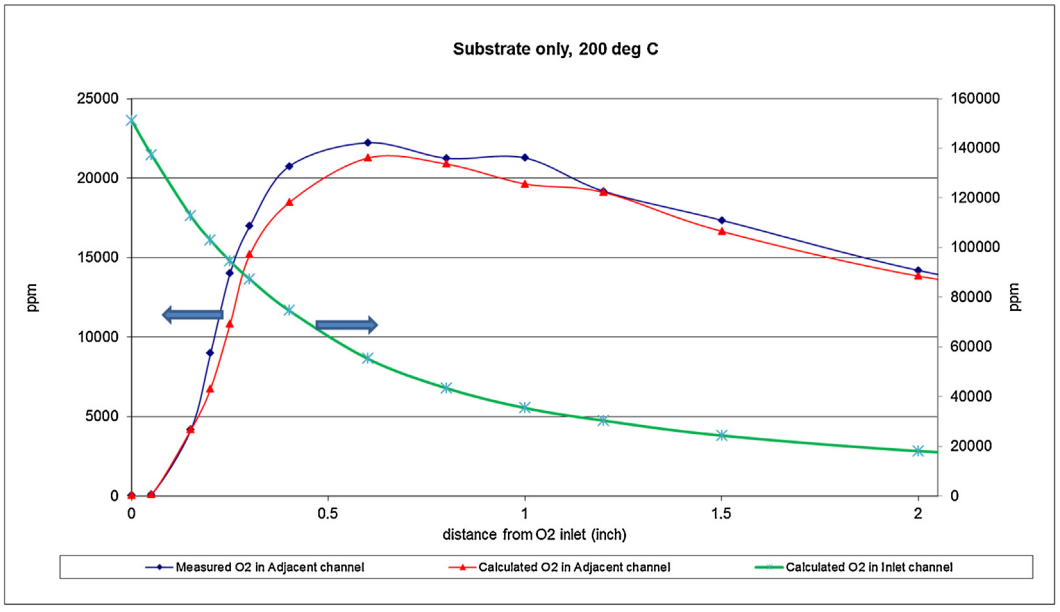

(b)

Fig. 7. ppm O_2 measured in the adjacent channel, calculated values in the adjacent and inlet channels of the substrate only sample at (a) 100 °C and (b) 200 °C vs axial distance from tracer gas inlet (inch).

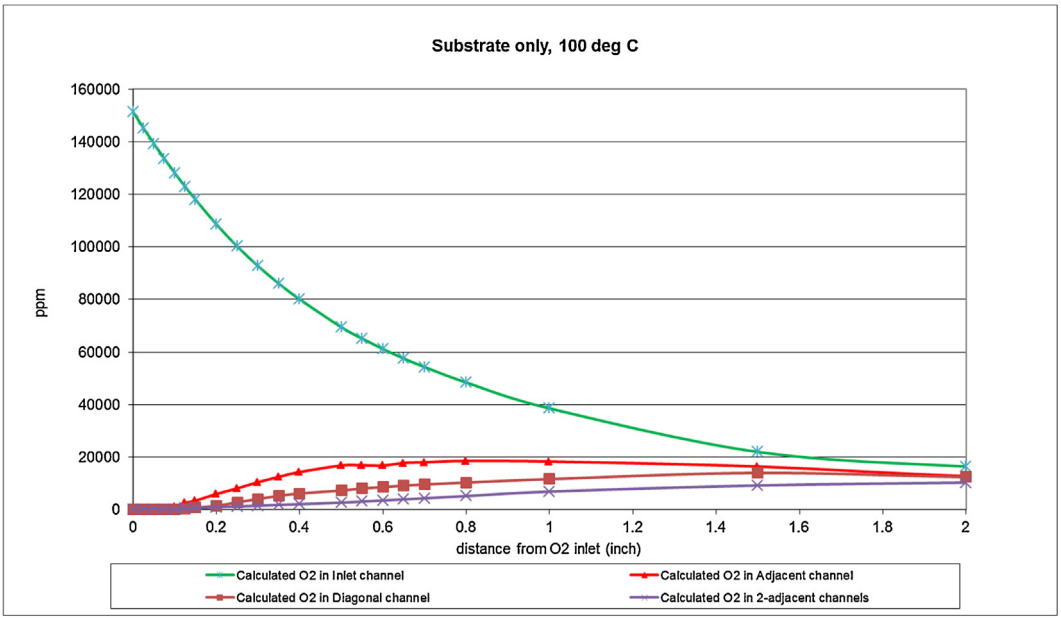

Fig. 8. ppm O_2 in the inlet, diagonal, adjacent and 2-adjacent channels (calculated values) of the substrate only sample at 100 °C.

Table 1
Monolith/Channel Parameters.

Monolith	300 cells per square inch, square channels.
Substrate thickness	282 μm
Washcoat 1 thickness	96.3 μm
Washcoat 2 thickness	62.7 μm
Bulk diffusivity of oxygen at 100 °C	1.9×10^{-5} m^2/s
Substrate porosity	65%
Washcoat porosity	32%

Table 2
Calculated Values/Results.

Diffusivity of O_2 (substrate) at 100 °C	9.28×10^{-6} m^2/s
Diffusivity of O_2 (substrate) at 200 °C	1.29×10^{-5} m^2/s
Temperature Dependence (Substrate)	$T^{1.4}$
Tortuosity of substrate	1.33
Diffusivity of O_2 (washcoat1) at 100 °C	2.21×10^{-6} m^2/s
Diffusivity of O_2 (washcoat1) at 200 °C	2.50×10^{-6} m^2/s
Temperature Dependence (washcoat1)	$T^{0.5}$
Diffusivity of O_2 (washcoat2) at 100 °C	2.20×10^{-6} m^2/s
Diffusivity of O_2 (washcoat2) at 200 °C	2.47×10^{-6} m^2/s
Temperature Dependence (washcoat2)	$T^{0.49}$

differences) is used to get the diffusivity in the substrate (D_{sub}) using Eq. (6).

5. The calculated inlet channel O_2 concentration and adjacent channel O_2 concentration (using the best $k_{overall}$ value) are shown in Fig. 7(a) (200 °C results in Fig. 7(b)).

Note that the concentration of O_2 in the various channels appears to converge at 2 in. length, see Fig. 8. Table 2 gives the calculated effective diffusivity of O_2 in the substrate at 100 and 200 °C. It also gives the substrate tortuosity value of 1.33, which is calculated using Eq. (1). Comparing the diffusivities at the two temperatures, diffusivity varies with $T^{1.4}$ which suggests that diffusion in substrate is bulk phase diffusion.

Once effective diffusivity of O_2 is known in the substrate, the same procedure (steps 1–5 shown above) can be repeated to get the effective diffusivity in the first washcoat layer using Eq. (7) for $k_{overall}$, and using data from Fig. 5(a) and (b). Note that D_{sub} is known from the calculations done for uncoated monolith. Calculated inlet channel O_2 concentration and adjacent channel O_2 concentrations, along with measured data in the adjacent channel, are shown in Fig. 9(a) and (b), at the two temperatures. Table 2 gives the effective diffusivity of O_2 in the first washcoat layer at 100 and 200 °C. From the data at the two temperatures, effective diffusivity varies with $T^{0.5}$, which is similar to Knudsen diffusion. Using the effective diffusivity values in the substrate and washcoat1, Eq. (8) can be used to calculate the effective diffusivity in the second washcoat layer for the dual layer sample (using data from Fig. 6(a) and (b)). Again steps 1–5 are followed, and D_{sub} and D_{wash1} are known from previous calculations. This will give information on how the diffusivity changes in the second washcoat layer and also how it scales with washcoat thickness. The results for the calculated inlet channel O_2 concentration and adjacent channel O_2 concentrations, along with measured data in the adjacent channels, are shown in Fig. 10(a) and (b), at the two temperatures for the dual (double) washcoat layer sample. Resulting data in Table 2 shows that the effective diffusivity in the second washcoat layer varies with $T^{0.49}$, which again suggests Knudsen diffusion. Comparing results for single and dual washcoat layers, it is confirmed that the diffusivities in

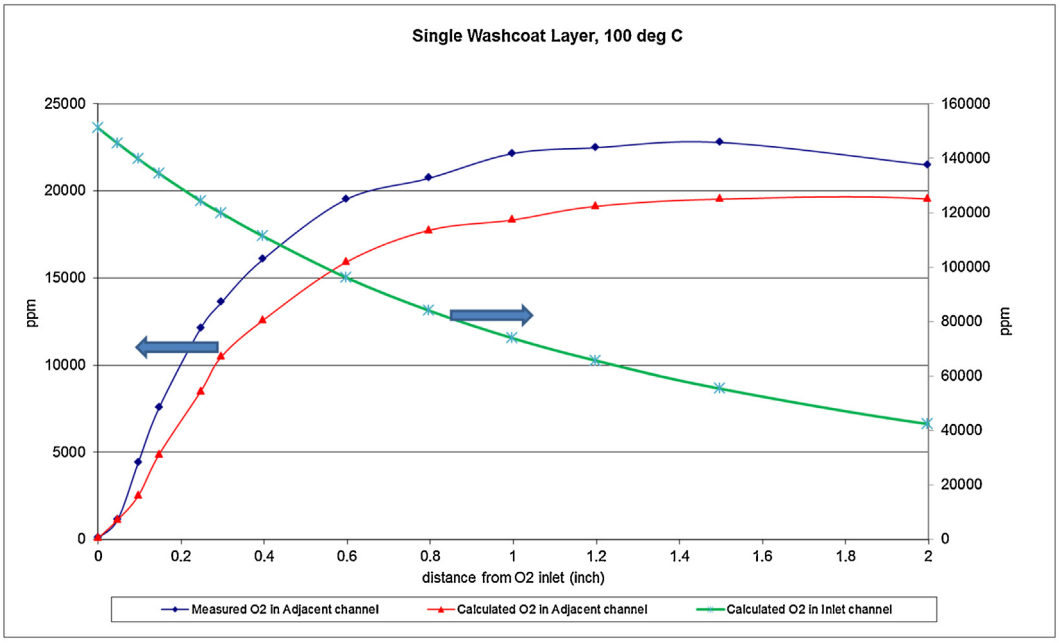

(a)

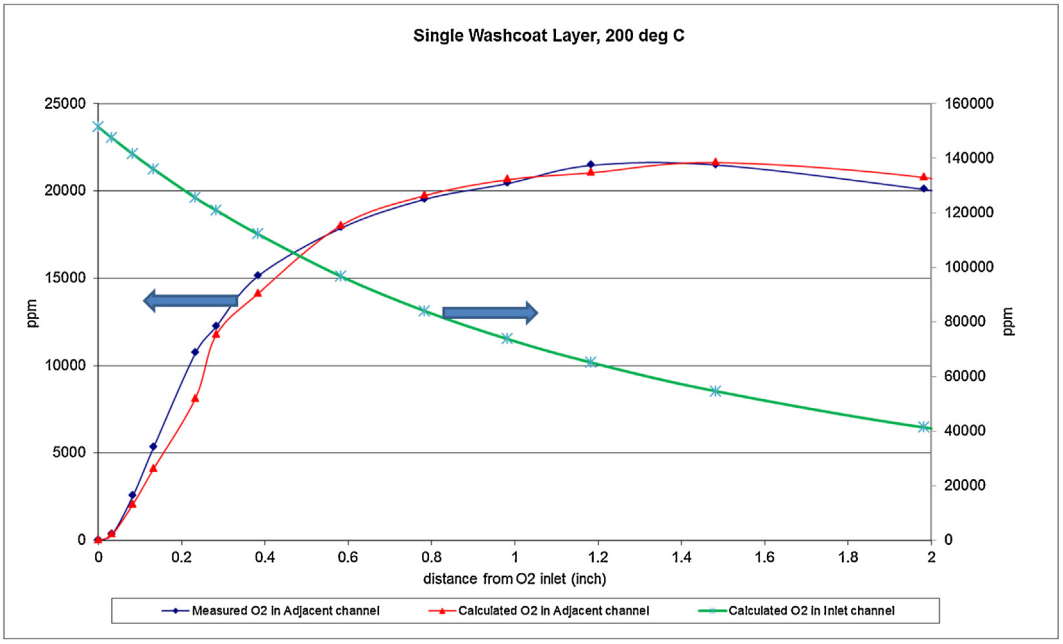

(b)

Fig. 9. ppm O_2 measured in the adjacent channel, calculated values in the adjacent and inlet channels of the single washcoat layer sample at (a) 100 °C and (b) 200 °C vs axial distance from tracer gas inlet (inch).

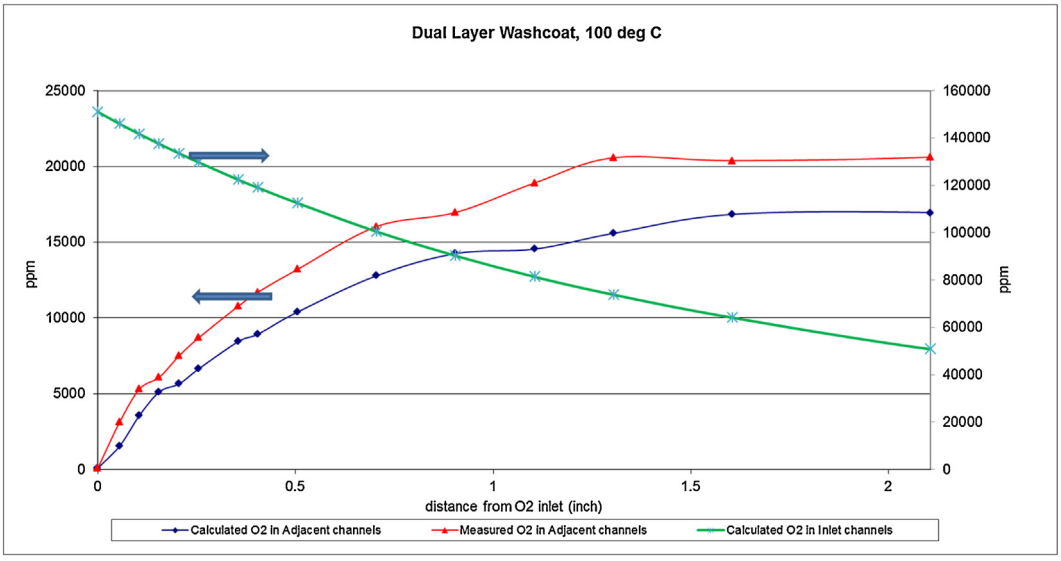

(a)

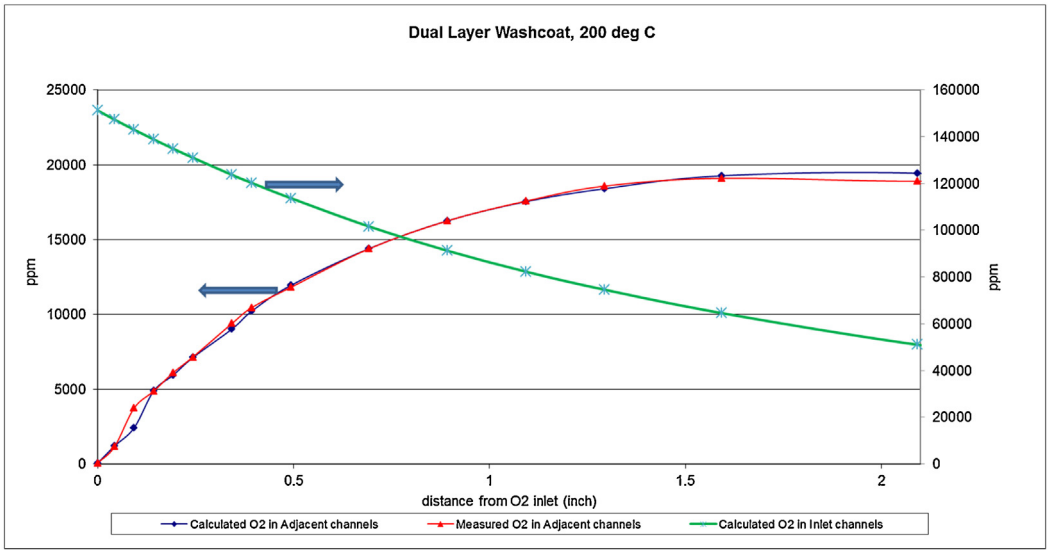

(b)

Fig. 10. ppm O_2 measured in the adjacent channel, calculated values in the adjacent and inlet channels of the dual washcoat layer sample at (a) 100 °C and (b) 200 °C vs axial distance from tracer gas inlet (inch).

the two washcoat layers are similar and suggest Knudsen diffusion regime for O_2 in the washcoat.

5. Conclusions

Valuable information can be obtained by measuring effective diffusivity in a porous catalyst. Calculated and measured diffusivities can be compared to obtain the tortuosity factor using Eq. (1). In this study a simple analytical method to measure effective diffusivity using the SPACI-MS technique, through the porous walls of a washcoated monolith, has been described. Effective diffusivity strongly depends on the structure of the porous catalyst. Diffusivity was measured for a substrate only, single washcoat layer and double washcoat layer monolithic catalyst. The substrate only experiments were used to measure the effective diffusivity of O_2 in the cordierite substrate of the monolith. Once the diffusivity in cordierite substrate was available, experimental data from single layer monolith was used to get the effective diffusivity of O_2 in the first layer of catalyst washcoat. Most of the monoliths for the automotive applications are dual layer. Thus a double layer monolith was used to get the effective diffusivity in the second layer, and also to see the effect of changing washcoat thickness on effective diffusivity measurements. It was found that the effective diffusivity of O_2 in the two layers was about the same. Experiments were performed at two temperatures (100 and 200 °C), to investigate the change in diffusivity with temperature. The effective diffusivity of O_2 in the substrate appears to follow bulk diffusion vs. temperature (varies directly with $T^{3/2}$), while for the two washcoat layers; the effective diffusivity follows Knudsen diffusion (varies directly with $T^{1/2}$). Experiments should be repeated at other temperatures to get a more accurate temperature dependence function.

This method has tremendous potential as a way of getting a quick estimate of the effective diffusivity in the porous washcoats

of catalytic monoliths, like the ones used for automotive applications. Presumably, the diffusivities in the monolith substrates (non-catalytic, constant porosity cordierite) would be more or less constant for monoliths of various sizes and cell densities. Also, most catalysts used for automotive applications use similar substrate material but different washcoat materials. Thus performing similar experiments on a washcoated monolith can provide the effective diffusivities in the newly designed porous washcoat directly (since substrate diffusivities would be known from previous experiments), which, as has been shown in this study, may scale with the washcoat thickness and layering. This method can also be used as a way of verifying and validating the theoretical models of mass transport through porous catalysts, by providing information on what kind of diffusion occurs at different temperatures, and also giving values of effective diffusivity to help in mathematical model development.

Finally, design of emissions control system architectures and control strategies increasingly rely on computer simulation tools, and the underlying models must account for mass transport to accurately predict catalyst performance over a wide range of conditions. Models require parameters that describe critical catalyst properties, including effective diffusivities. Typically model developers have to resort to order of magnitude estimates for diffusivities, often based on experimental measurements conducted on loosely related materials, or else leave mass transport coefficients as tunable parameters in their models. This paper, which provides reliable measurements of diffusivities through relevant materials under appropriate conditions, provides a key piece of information for emissions control device model developers. Further, the method described in this paper could be repeated by other researchers to build a library of reference mass transport parameters. Therefore, this study is also an attempt to make a contribution to the state of knowledge for catalytic emissions control devices.

References

[1] N. Wakao, J.M. Smith, Diffusion in catalyst pellets, Chem. Eng. Sci. 7 (1962) 825–834.
[2] T. Richardson James, Experimental determination of catalyst fouling parameters: diffusivity, Ind. Eng. Chem. Process Des. Dev. 11 (1972) 12–14.
[3] W. Beeckman Jean, Measurement of the effective diffusion coefficient of nitrogen monoxide through porous monolith-type ceramic catalysts, Ind. Eng. Chem. Res. 30 (1991) 428–430.
[4] R.E. Hayes, S.T. Kolaczkowski, P.K.C. Li, S. Awdry, Evaluating the effective diffusivity of methane in the washcoat of a honeycomb monolith, Appl. Catal. B: Environ. 25 (2000) 93–104.
[5] J.S. Choi, W.P. Partridge, W.S. Epling, N.W. Currier, T.M. Yonushonis, Intra-channel evolution of carbon monoxide and its implication on the regeneration of a monolithic Pt/K/Al2O3 NOx storage-reduction catalyst, Catal. Today 114 (1) (2006) 102–111.
[6] Marco Dondero, Adriaín P. Cisilino, J. Pablo Tomba, Experimental validation of computational models for mass transport through micro heterogeneous membranes, J. Membr. Sci. 437 (2013) 25–32.
[7] Kotaro Akashi, Kaori Inoue, Masayuki Adachi, Kozo Ishida, Johannes Villinger, Werner Federer and Albert Dornauer, Utilization of a soft ionization mass spectrometer for ultra-high sensitivity and fast response emission measurement, SAE paper 980046.
[8] Gunda Millonig, Siegfried Praun, Michael Netzer, Christian Baumgartner, Albert Dornauer, Sebastian Mueller, Johannes Villinger, Wolfgang Vogel, Non-invasive diagnosis of liver diseases by breath analysis using an optimized ion-molecule reaction mass spectrometry approach: a pilot study, Biomarkers 15 (4) (2010) 297–306.